5000 groove/mm multilayer-coated blazed grating with 33% efficiency in the 3rd order in the EUV wavelength range

Dmitriy L. Voronov,*[a] Erik H. Anderson,[a] Rossana Cambie,[a] Farhad Salmassi,[a]
Eric M. Gullikson,[a] Valeriy V. Yashchuk,[a] Howard A. Padmore,[a]
Minseung Ahn,[b] Chih-Hao Chang,[b] Ralf K. Heilmann,[b] Mark L. Schattenburg[b]
[a]Lawrence Berkeley National Laboratory, 1 Cyclotron Road, Berkeley, CA 94720
[b]Space Nanotechnology Laboratory, Massachusetts Institute of Technology, 70 Vassar St., Cambridge, MA 02139

ABSTRACT

We report on recent progress in developing diffraction gratings which can potentially provide extremely high spectral resolution of 10^5-10^6 in the EUV and soft x-ray photon energy ranges. Such a grating was fabricated by deposition of a multilayer on a substrate which consists of a 6-degree blazed grating with a high groove density. The fabrication of the substrate gratings was based on scanning interference lithography and anisotropic wet etch of silicon single crystals. The optimized fabrication process provided precise control of the grating periodicity, and the grating groove profile, together with very short anti-blazed facets, and near atomically smooth surface blazed facets. The blazed grating coated with 20 Mo/Si bilayers demonstrated a diffraction efficiency in the third order as high as 33% at an incidence angle of 11º and wavelength of 14.18 nm. This work was supported by the US Department of Energy under contract number DE-AC02-05CH11231.

Keywords: blazed grating, multilayer, EUV, soft x-rays, scanning interference lithography, anisotropic etch, microfabrication

1. INTRODUCTION

High groove density and high-efficiency diffraction gratings are required for high-resolution soft x-ray spectroscopy[1] and EUV astrophysics.[2] Blazed gratings coated with a multilayer (ML) are most promising because they potentially concentrate almost all the diffracted energy into the order of interest. They are, however, more difficult to fabricate because they demand very high quality of the saw-tooth substrate. Grating fabrication processes should provide both precision control of the groove profile and low roughness of the groove surface. Despite the great recent progress in saw-tooth grating fabrication techniques, the efficiency of the gratings reported so far is still significantly below theory. The best EUV blazed gratings are fabricated with interference lithography combined with ion-beam etching[3,4] and gray-scale e-beam lithography.[5] Recent progress of these techniques has allowed to achieve a diffraction efficiency of 36.2% at the wavelength of 13.62 nm with a grating with the groove density 2400 grooves/mm optimized for diffraction in the second order.[6] A denser 3000 grooves/mm grating has demonstrated efficiency in the second order diffraction of 29.9% at the wavelength of 15.79 nm.[3] Efficiency of 41% has been obtained in 1st order diffraction at the wavelength of 12.5 nm with a 1000 groove/mm grating fabricated with the gray scale e-beam exposure method.[5] The examples above show that the technological difficulties increase with higher groove densities and blaze order number, which are necessary to get high dispersion and spectral resolution.

The level of the groove surface smoothness of 0.5-1 nm rms achieved in the works cited above is acceptable for EUV (the wavelengths of 13 nm and longer) applications. For shorter wavelength much smoother surfaces are required, and that seems to be a problem for these techniques. Wet anisotropic etch of silicon single crystals looks like a more promising technique for blazed grating fabrication. The anisotropic etch can potentially provide a super-smooth surface with a roughness as small as 0.1 nm.[7] The technique is based on the high selectivity of silicon etching with alkali solutions for {111} crystallographic planes, which are etched slower by factor 100-400 than other ones. This technique

*dlvoronov@lbl.gov; phone 1 510 486-4863; fax 1 510 495 2591

Advances in X-Ray/EUV Optics and Components IV, edited by Ali M. Khounsary, Christian Morawe, Shunji Goto,
Proc. of SPIE Vol. 7448, 74480J · © 2009 SPIE · CCC code: 0277-786X/09/$18 · doi: 10.1117/12.826921

was suggested in Ref.[8] for infrared gratings and then successfully applied for grazing incidence hard x-ray blazed gratings.[9] The small surface roughness is crucial for soft x-ray blazed gratings. First attempt to fabricate a ML coated blazed grating for the water window showed how difficult it is to realize the advantages of an anisotropic etch approach.[10] A thorough optimization of the etch process and grating design is necessary. In this paper we report our first results of such an optimization. We describe an EUV blazed grating which combines a high groove density and high diffraction efficiency in the 3rd blazed order.

2. EXPERIMENT

The saw-tooth gratings were fabricated by anisotropically etching a silicon wafer with an aqueous solution of KOH. A float zone silicon wafer with resistivity of 6000 Ohm cm was used. The surface of the wafer was close to (111) plane, but had a 6-degree miscut towards the $[11\bar{2}]$ direction. The miscut provided a 6 degree angle between the surface and (111) planes. The wafer was covered by 20-30 nm of low-stress CVD silicon nitride. The grooves of the subsequently applied grating pattern should be parallel to the (111) planes on the wafer surface. The main flat of the wafers can serve just as a preliminary reference for the in-plane wafer orientation. In order to find a more exact wafer orientation a preliminary KOH etch of a fan pattern was applied similar to Ref.[11] The fan pattern consists of spoke-like rectangular openings which have different in-plane rotations. The openings are made in the nitride by contact photolithography and RIE plasma etch. Then a KOH etch was applied, that results in etching of trenches in the wafer. The etching of trench sidewalls produces an undercut of the nitride coating, which can be measured with a Scanning Electron Microscope (SEM). The larger the inclination of the sidewalls from {111} planes, the faster is the sidewall etch rate and the larger is the nitride undercut. The minimum undercut found by fitting of the undercut data versus the rotation angle of the trenches by a second order polynomial shows the direction of intersection of the {111} planes and the wafer surface. The minimum undercut direction was used as a reference for orientation of a periodic line pattern with a pitch of 200 nm. The pattern was produced with scanning interference photolithography using the state-of-art Nanoruler instrument available at MIT.[12] The parameters of light exposure of the photoresist were optimized to obtain the duty-cycle ratio of 0.25-0.3. After reactive-ion etch (RIE) of the antireflective coating and the nitride, the wafer was cleaned and cut in small samples which were used for KOH etch optimization. The grating sample discussed in this paper has a size of $6\times8mm^2$. The wet etch of a sample was performed at room temperature and at a KOH concentration of 20% with intensive agitation of the solution. After the KOH etch finished, the nitride mask was removed and the sample was cleaned in order to prepare for surface characterization.

Groove profile and groove surface quality were characterized with a Dimension 3100 Scanning Probe Microscope (SPM) operating in tapping mode. Silicon probes with a nominal tip radius of 7 nm were used. Scanning was performed in both parallel and perpendicular directions relative to the grating grooves. The parallel scans (scan lines are parallel to the grating grooves) were used for surface roughness measurements. The SPM images were flattened on a line-by-line basis: a first-order polynomial was subtracted from each line in order to compensate an average slope of the image and bring all lines to the same height to compensate the 6-degree slope of the facets. The roughness of the groove surface was calculated for an entire area of a $1\times1\ \mu m^2$ flattened image, the nub and anti-blazed facet areas which suffer from artifacts when such a kind of flattening is applied were excluded from the calculation. Note, line-by-line flattening makes facets flat, and information about the real groove profile is lost in this way. In order to measure the grating profile, the perpendicular scans (scan lines perpendicular to the grating grooves) were performed. A first order polynomial was subtracted from the entire image to compensate an average slope of the image. The blaze and anti-blaze angles of the gratings were measured by averaging all of the lines of each image followed by a linear fit of the facet surface.

The multilayer coating composed of 20 Mo/Si bilayers was deposited on the nub-free (see details below) blazed grating substrates by dc-magnetron sputtering. Simultaneously, a witness multilayer mirror was deposited on a flat silicon wafer. In order to provide a uniform thickness of the coating, the deposition was performed by moving with a constant-rate the substrates over a source aperture designed to provide a uniform thickness of the coating on a substrate. The multilayer period of 7.24 nm was desired in order to provide the Bragg condition for the blazed wavelength of the grating with 200 nm period and the grating angle of 6 degrees. The optimal period of the multilayer was estimated from the grating equation and the Bragg condition, taking into account refraction:[13]

$$\frac{d_{grating}\sin\phi}{D_{ML}\sqrt{1-\frac{2\delta-\delta^2}{\sin^2\theta}}}=\frac{m}{n},$$

where $d_{grating}$ is a grating period, ϕ is the blaze angle, D_{ML} is a multilayer period, δ is an increment of a real part of the refraction index of the multilayer, θ is a Bragg angle, m is the grating order, and n is the multilayer Bragg order.

In order to minimize deposition of the multilayer on the anti-blazed facets, the grating substrate was not strictly placed against the center of the magnetron source, but it was off-center by 35 mm. Here we took into account the fact that the topography translates along the average direction of an incident atomic flux that was observed in Ref.[14] for binary phase multilayer gratings.

The total thickness of the 20-period multilayer is 145 nm which is close to the width of the grating facets. Note, that a twice thicker multilayer is necessary to get the highest possible reflectivity. However, for the thicker multilayer we would expect a reduction of grating efficiency due to perturbation of the structure of the multilayer stack caused by distortion of the grating profile, deposition of the materials on the anti-blazed facets, etc. It is difficult to predict what part of the 200 nm groove will be affected, but the perturbation will be evidently increased with increase of the multilayer thickness. In order to minimize the perturbation effects in the pilot experiment described here, we choose the thickness of the multilayer to be reduced.

Efficiency measurements were performed at ALS beamline 6.3.2, ALS. The incident angle was set to 5º for the flat witness, and 11º for the grating (that corresponds to 5º angle between incident ray and 6-degree groove surface). The detector slit with size of 0.5 mm provided the angular resolution of 0.12º. On the other hand the slit was still wider than the beam, which insures the correct efficiency measurements. The detector scans over the diffraction angle were performed at the wavelengths between 13.4 nm and 15.0 nm with an increment of 0.1 nm. The data were normalized to the direct beam measured over the wavelength range. Also a wavelength scan with the witness sample was performed in order to determine the resonance wavelength of the multilayer.

3. RESULTS AND DISCUSSION

The SEM image and SPM profile of the grating after KOH etch are shown in Fig.1. High etch selectivity to the {111} planes provides well shaped 6-degree blazed facets of the grating. The anti-blazed facets are tilted by more than 65º and occupy about 5% of the length of a groove. This is much better than what has been achieved with the competitive techniques of fabrication of blazed gratings. The main imperfections of the anisotropically etched grating are the silicon nubs seen in the upper part of the grooves (Fig. 1). They are shaped with {111} sidewalls and the top surface, which is the original surface of the silicon wafer covered with the nitride mask during the KOH etch. The width of the nubs is 15-20 nm and the height is about 30 nm. The nubs are undesirable features of the grating profile since they can lead to shadowing the atomic flux during the coating deposition and result in significant perturbations of the multilayer structure. Such a perturbation that occupied a significant portion of the grooves of a 10 μm period grating was one of the main reasons for efficiency losses in Ref.[15] For a 200 nm grating the nubs cannot be tolerated at all because the thickness of a multilayer is comparable to the grating period and the corresponding perturbation of the multilayer structure would be large.

A chromium deposition followed by a lift-off process was applied earlier[8] in order to remove the nubs. This technique produces trenches instead of nubs which are much better from the point of view of the shadowing problem. Here, in order to obtain a nub-free triangle profile of the grooves, we tried a few different approaches all based on the oxidation of silicon. First, we tried a silicon thermal wet oxidation performed at the temperature 800ºC and followed by an oxide etch with 49% hydrofluoric acid. This technique was found to result in rather curved facets and, therefore, it was rejected. A better result was obtained with a multiple-step procedure consisting of chemical oxidation alternated by etching the grown oxide. In each step, the surface of the silicon grating was first oxidized with Piranha (a heated mixture of sulfuric acid and hydrogen peroxide) and then the oxide was etched out with hydrofluoric acid. A silicon oxide layer with thickness of 1-2 nm should grow and be removed during a cycle; the process consumes 0.5-1 nm of the silicon. Because initially the nub width is about 15-20 nm, after 10-15 oxidation/etch cycles the nub sidewalls meet each other and the nubs collapse. Finally, the profile of the grating groove approaches an ideal triangle shape, though some residual nub features can be still observed in the SPM profiles after 15 cycles (Fig. 2b).

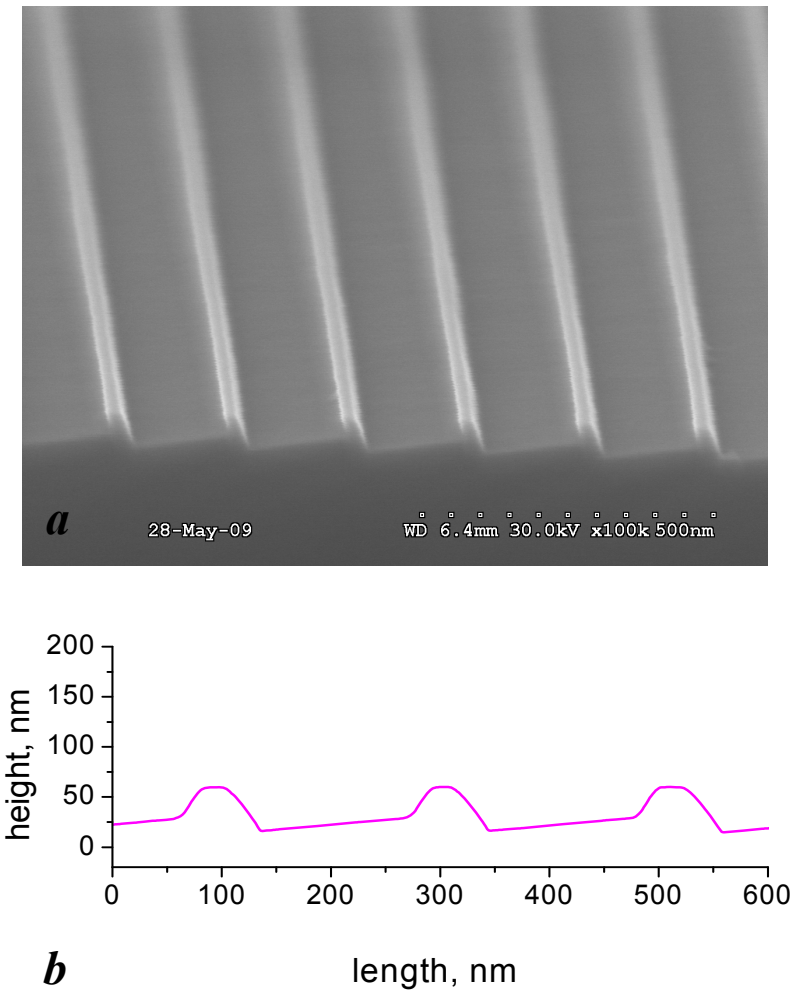

Fig. 1. A SEM image (a) and an SPM profile (b) of the 200 nm grating after KOH etch and nitride mask removal. There are silicon nubs which should be removed before ML deposition. The width of the nubs is 15-20 nm, the height is about 30 nm.

The SPM images shown in Fig. 3 give an idea how the morphology of the groove surface changes after each technological step discussed above. After the KOH-etch step, the surface consists of horizontal atomically smooth terraces (each of them has its own color) which are (111) planes and atomic steps. This kind of morphology is an inherent feature of the step-flow mechanism of anisotropic etching,[15] when the (111) terraces are relatively stable to the etchant when compared with the atomic steps; and the etch predominantly occurs as a motion of the atomic steps. There are 40-50 steps over a one-micron SPM trace (see the SPM profile in Fig. 3a), therefore, an average width of a terrace is about 25 nm. From our previous experience,[16] we know that low groove density gratings with a period of 4-10 microns suffer from significant curvature of the groove surface. We found that this imperfection is caused by a non-uniform distribution of the step density across a 2-8 micron facet of the gratings. It is not still clear why the distribution is not uniform, and how to obtain a flat surface. In order to bypass the problem we shifted to the 200 nm period gratings which were expected to be free of the groove curvature. Across a single (~200 nm) facet, there are just a few steps, and their positions are rather random. The perturbation of the facet surface by the randomly distributed steps is described with the surface roughness rather than with systematic distortion of the groove profile. This is confirmed with the SPM measurements of the grating profile (Fig. 1). The measurements do not show any significant variation of the blaze angle

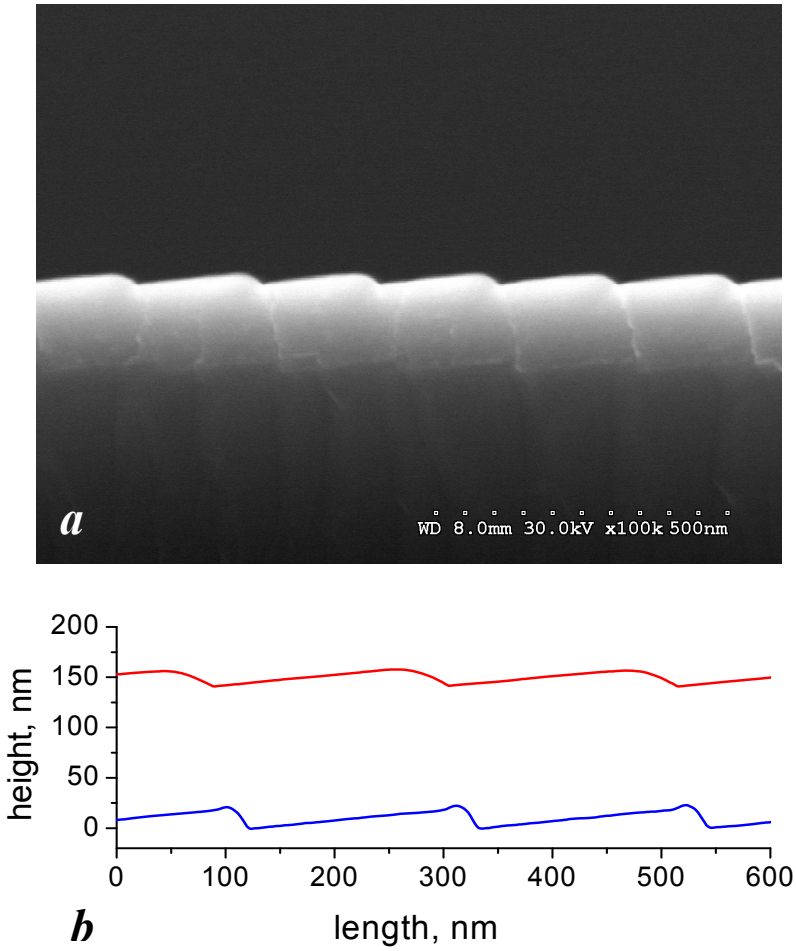

Fig. 2. Cross-section image (a) and SPM profiles (b) of the nub-free 200 nm grating coated with Mo/Si multilayers composed of 20 bilayers. Both before and after deposition profiles of the grating are shown by lower and upper curved respectively.

across the groove. The surface roughness measured over 1×1 μm^2 varies from scan to scan within the range of 0.25-0.28 nm rms.

After the nub removal procedure the groove surface significantly changes (Fig. 3b). There is not a step-flow morphology anymore; it is replaced by a granular morphology. This fine granulation evidently increases the high frequency surface variation, and the SPM measurements yield a surface roughness of about 0.4 nm rms for a 1×1 μm^2 scan. Other serious surface imperfections are nano-pits which are 30-50 nm wide and a few nanometers deep. The best samples have a relatively small number of the pits (just a couple of them are seen in Figs. 3b and 3c), so their contribution in the total surface roughness is minor. However, the nano-pits are difficult to control; they tend to multiply and increase in size with a number of the oxidation cycles. The nano-pit problem is probably related to the purity of the silicon surface during the process of chemical oxidation and requires further optimization of the nub removal step. Note that similar nano-pits were observed after a RCA-1 clean of silicon wafers,[17] and the authors used the same Piranha/HF cycles to remove the pits.

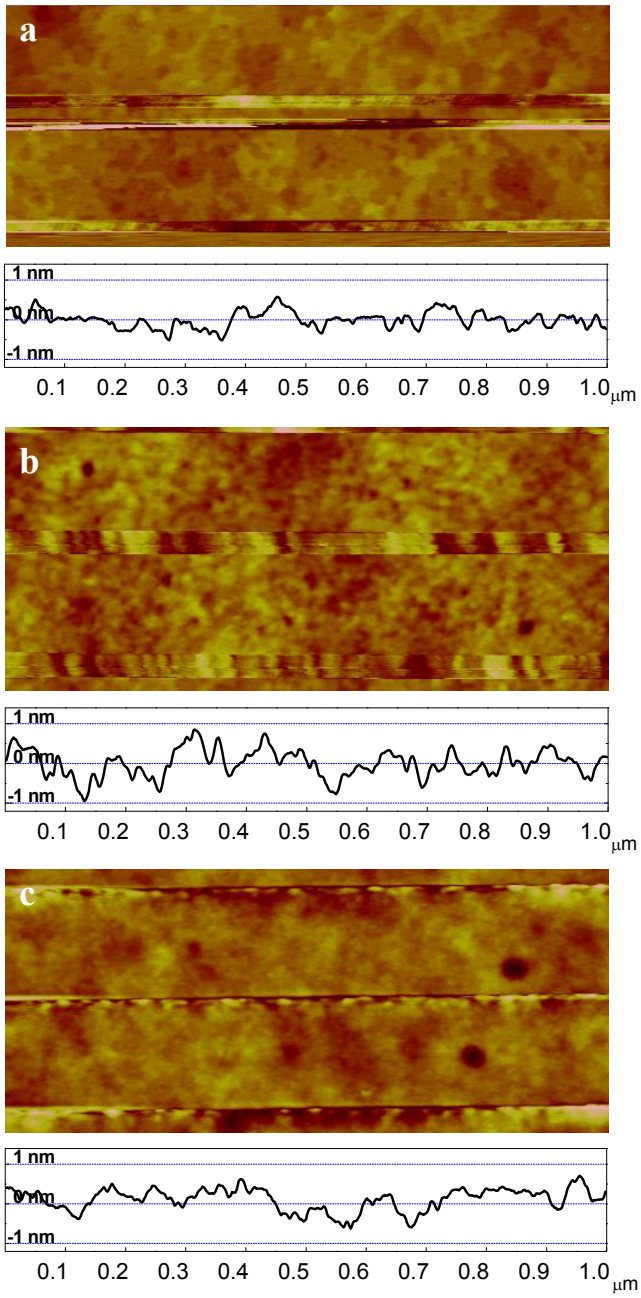

Fig. 3. Morphology of the groove surface of the 200 nm grating after KOH etch (a), nub removal (b), and multilayer deposition (c). The typical SPM profiles are also shown to illustrate the surface height distribution in the direction parallel to the grooves.

Deterioration of surface smoothness might be an inevitable drawback of the oxidation approach. We switched from a highly anisotropic KOH etch, which is a powerful tool providing smoothing of the high-frequency roughness, to a rather isotropic process of silicon oxidation. If further investigation confirms this point, the oxidation approach will probably not work for soft x-ray gratings, and should be replaced by a more efficient one which would provide both a triangle profile of the grooves and good quality of the facet surface. For EUV gratings the obtained roughness is quite tolerable since it does not significantly affect the grating efficiency as it is shown below. Moreover, the high frequency component of the surface roughness introduced by the nub removal step can be partially smoothed by the multilayer

deposition. Indeed, some improvement of the surface is observed after the multilayer deposition: the roughness of the groove surface of the grating coated with the multilayer is 0.3-0.35 nm rms (Fig. 3c). The multilayer smoothes the high special frequency features, such as a fine granulation, but the larger defects, like nanopits, are still well visible.

The smoothing ability of the multilayer is vital for surface roughness suppression, but it adversely affects the grating profile. The profile change is well visible on the cross-section SEM image as well as in the SPM traces in Fig. 2. The surface of the blazed facets gets slightly convex. The apexes of the triangle grooves are significantly smoothed and rounded. Since they are high-frequency features of the gating profile, they are mostly affected by the smoothing. The geometry of the deposition setup can also cause a change of the grating profile. Because of the large size of the magnetron source, the atoms arrive to the substrate from a wide solid angle. This causes a deposition of the material on the anti-blazed facets and promotes rounding of the apex. As a result of the smoothing processes, the anti-blazed facet gets rather curved and its average slope angle reduces from 64º before the deposition to 25-30º after the deposition. At the same time the areas at the bottom of the blazed facets appeared to be partially shadowed. The shadowing effect which predominates over the smoothing of these high frequency profile features results in small troughs in the bottom part of the grooves.

The profile changes seen in the upper and the bottom part of the facets cause undesirable perturbation of the multilayer because of local variation of the blaze angle and/or period of the multilayer. The perturbed area occupies approximately 25-30% of a 200 nm facet. As it was mentioned above, the rounding effect is probably due to the specific geometry of the multilayer deposition and due to surface migration of the deposited atoms. Note that the deposition geometry can be significantly improved by using strongly collimated atomic beams, for example, ones obtained by ion-beam sputtering. However, a complete suppression of the rounding effect seems to be impossible due to the fundamental character of the surface mobility of the deposited atoms. This means a fundamental limitation for groove density of ML blazed gratings, because the shorter period of the grating the larger portion of a ML facet is perturbed.

This limitation can be overcome with the method suggested in Ref.[18] and firstly realized in Ref.[16] The method is based on the sliced grating approach developed by the authors[19,20] earlier. According to the method, a blazed ML grating fabricated by deposition of a soft x-ray multilayer on a low groove density saw-tooth substrate is additionally polished removing part of the coating. The polishing forms an oblique-cut multi-line structure that is a sliced multilayer grating. The resulting grating has a short-scale periodicity of lines, which is defined by the multilayer period and the oblique-cut angle. The total number of lines of the original ML sliced grating[19,20] is limited by the total thickness of the multilayer. In the method used in Ref.[15,19], the limitation is overcome by using a blazed grating substrate coated with a reasonably thin multilayer. Note that in contrast to a 200 nm ML blazed grating, the portion of the sliced grating perturbed by the atomic mobility effect is significantly reduced, and one can expect efficiency improvement providing the facet curvature problem would be solved. In spite of the fact that the present work is mostly devoted to the development of a high quality ML blazed grating, the investigation is a part of the more broad research and development program that also includes optimization of the processes to fabricate super high density sliced multilayer gratings suitable for soft x-ray applications.

Returning to the grating profiles shown in Fig. 2, the positions of the apexes of the multilayer are quite different from the position of the tooth top edges of the grating substrate. The apexes are shifted to the left in Fig. 2a corresponding to the direction of the multilayer growth that should be parallel to the average direction of the atomic flux from the magnetron source. The observed direction of the ML growth is qualitatively consistent with the average direction of the atomic flux; however, there is some quantitative difference. In the course of the ML deposition, the atomic flux was directed at an angle of approximately 20º in respect to the direction normal to the substrate surface. That is noticeably different from the observed angle of apex shift of about 12.º Moreover, the angle of apex shift is not constant and seems to increase with the multilayer thickness. In any case, the observation shows that the apex shift can be controlled by the adjustment of the sample and therefore can be optimized in the future in order to get higher grating efficiency.

The diffraction efficiency of the multilayer coated blazed grating was measured at ALS beamline 6.3.2. At the incident angle of 11º, the blazed wavelength of the incident light was found to be 14.18 nm. Figure 4 shows a detector angle scan recorded with this wavelength fixed. The efficiency of the 3rd inner order is more than 33%. Total efficiency of all other observed orders does not exceed 4%. The 5th and higher positive orders can not be observed because the detector blocks the incident beam. The 2nd and 4th orders are almost equally suppressed; this is a signature of an optimal ratio of the grating and multilayer periods, when the maxima of the multilayer bandwidth and the groove diffraction function are matched. The 3rd blazed order rests on a background of diffuse scattering due to the roughness of the facet surface. The signal-to-noise ratio is 10^3, confirming the very good quality of the grating.

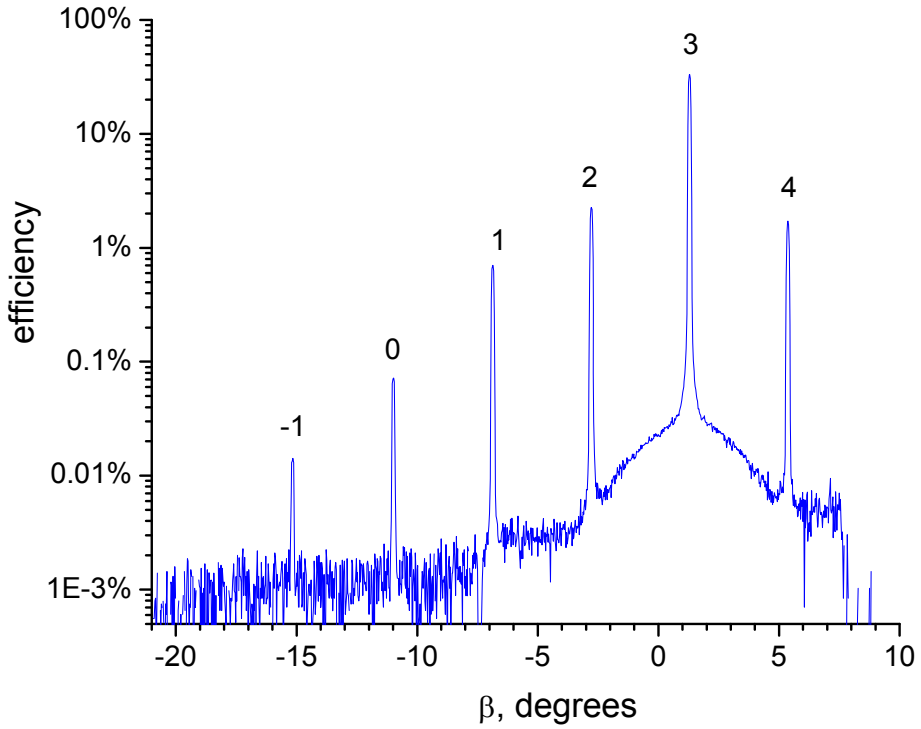

Fig. 4. Efficiency of the multilayer coated grating measured at the incidence angle of 11º and the wavelength of 14.18 nm.

Figure 5 shows the dependence of the efficiency of the 3rd positive order with respect to wavelength. The dependence was obtained from a series of the detector angle scans, similar to one shown in Fig. 4, performed at different wavelengths. A wavelength scan with the witness ML mirror performed at the incident angle of 5º measured from the normal is also shown. The angle corresponds to the grating incident angle α=11º accounting a 6-degree blaze angle. Both curves have a very similar shape because the working wavelength range of the multilayer coated grating is determined by the bandwidth of the multilayer reflector. The reflectivity of the witness mirror is higher than 52%; therefore, the grating groove efficiency is about 63%. We believe that the perturbations of the multilayer caused by rounding discussed above are the main reason of the reduction of the groove efficiency. The perturbed portion of a groove of 25-30%, leading to a direct loss of grating efficiency, roughly explains the measured efficiency. An additional impact of the perturbations on the grating efficiency is due to a change of the groove diffraction function. For an ideal grating with no perturbations, the facet length would be equal to the grating period. In this case the minima of a groove diffraction function would coincide with the position of diffraction orders (except for the blazed order), and all orders neighboring to the blazed one would be suppressed. However, because of perturbations the working part of the facet decreases and that means the facets get narrower. It results in a wider groove diffraction function; the minima of the groove function and the positions of the diffraction orders do not coincide anymore, and the orders appear to be not suppressed completely. Hence, some part of the diffraction energy is directed into the non-blazed orders and the efficiency of the blazed order reduces.

The performed measurements suggest that the geometrical perturbations of a ML blazed grating significantly affect the grating diffraction efficiency even at the EUV energy range when the grating operates close to normal incidence. For a soft x-ray grating, the problem can be much more severe because the grating would operate at grazing incidence. In this case the incident and reflected radiation will pass the perturbed areas and, therefore, suffer from additional absorption. The minimization of the perturbed areas seems to be one of the main issues in making further progress. One can possibly take advantage of an increase in the grating period, since this would reduce the relative portion of the perturbed areas.

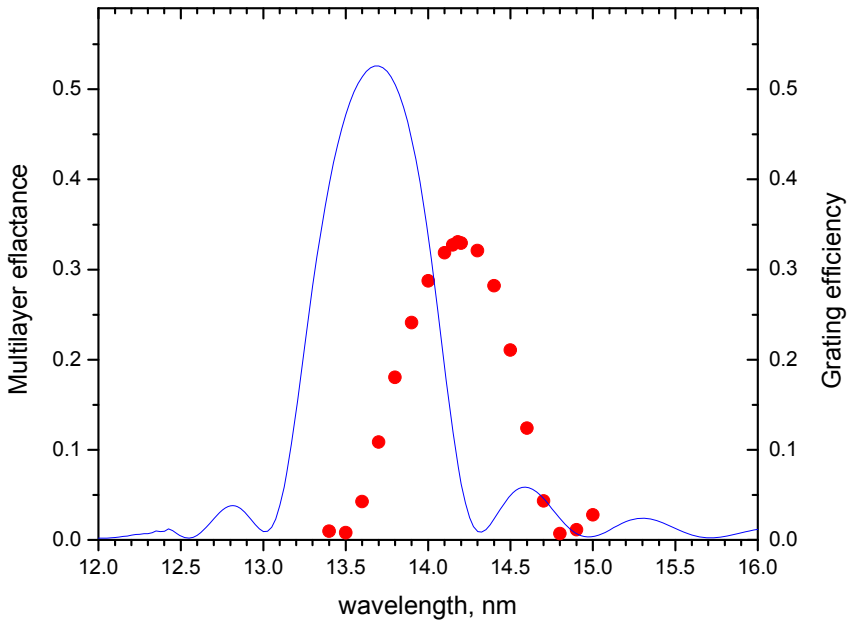

Fig. 5. Wavelength dependence of efficiency of the 3rd order of the grating (dots) and multilayer witness reflectance (line).

Figure 5 shows that the resonance wavelength is different for the grating and the witness multilayer. Since the grating blaze condition is determined by the multilayer bandwidth, the shift of the resonance wavelength means that the period of the multilayer deposited on the 6-degree tilted grating facets is 4% larger of that of the witness mirror. The difference can be explained by the fact that the magnetron aperture was optimized for a flat substrate rather than for a saw-tooth surface. A coating deposited without the aperture would have a dome-like radial distribution of thickness, partially due to variations of the angle between the average atomic flux and the substrate. The shape of the aperture is optimized to compensate the flux angle variation by increasing the exposure time of peripheral areas of a 4-in substrate, and provide in this way a uniform thickness of the coating. The grating has 6 degree tilted facets, and the flux angle distribution is rather different from that for a flat substrate. The existing aperture does not provide the right thickness compensation throughout a saw-tooth substrate area. For a small sample the ML period depends on the sample position, and can be larger or smaller than the period of a flat ML witness. In the case of the grating discussed here the aperture results in a 3-4% increase of the multilayer period. The ML period variation over the grating area was estimated to be less than 1%, but for larger gratings the optimization of the aperture is required.

4. CONCLUSIONS

A high quality blazed grating was fabricated by scanning interference lithography and anisotropic KOH etching of silicon. The optimized anisotropic etching of short-period gratings provides excellent control of the slope of grating facets which are completely free from curvature, have an ultra high smoothness of groove surface, and a very steep angle of anti-blazed facets. Following the technological steps of nub removal and multilayer deposition result in some mild deterioration of the grating and require some additional optimization. Achieved performance of the grating fabrication process provides the efficiency of a multilayer coated grating as high as 33% even with a half-thick Mo/Si multilayer. The 200 nm period grating operating in 3rd blazed order has a very high dispersion equal to one for a first order grating with the groove density of 15,000 grooves/mm. The high potential of the described techniques provides an optimistic outlook for fabrication of ultra-dense and ultra-high resolution soft x-ray gratings. It should also be mentioned that calculations have shown that very high diffraction efficiency can be achieved in almost arbitrarily high order, if the grating can be made perfect enough.

ACKNOWLEDGEMENTS

The authors are very thankful to Wayne McKinney and Yegor Bugaev for useful discussions, and invaluable assistance.

The Advanced Light Source is supported by the Director, Office of Science, Office of Basic Energy Sciences, Material Science Division, of the U.S. Department of Energy under Contract No. DE-AC02-05CH11231 at Lawrence Berkeley National Laboratory.

DISCLAIMER

REFERENCES

[1] Workshop on "Soft X-Ray Science in the Next Millennium: The Future of Photon-In/Photon-Out Experiments. (Pikeville, Tennessee March 15–18, 2000), http://www.phys.utk.edu/WPWebSite/ewp_workshop_XRay_Report.pdf

[2] Kowalski, M. P., Barbee, Jr., T. W. and Hunter W. R., "Replication of a holographic ion-etched spherical blazed grating for use at extreme-ultraviolet wavelengths: efficiency," Appl. Opt. 45(2), 322-334 (2006).

[3] Kowalski, M. P., Cruddace, R. G., Heidemann, K. F., Lenke, R., Kierey, H., Barbee, Jr., T. W. and Hunter, W. R., "Record high extreme-ultraviolet efficiency at near-normal incidence from a multilayer-coated polymer-overcoated blazed ion-etched holographic grating," Opt. Lett. 29(24), 2914-2916 (2004).

[4] Lin, H. and Li, L., "Fabrication of extreme-ultraviolet blazed gratings by use of direct argon–oxygen ion-beam etching through a rectangular photoresist mask," Appl. Opt. 47(33), 6212-6218 (2008).

[5] Naulleau, P. P., Liddle, J. A., Anderson, E. H., Gullikson, E. M., Mirkarimi, P., Salmassi, F. and Spiller, E., "Fabrication of high-efficiency multilayer-coated gratings for the EUV regime using e-beam patterned substrates," Opt. Comm. 229, 109–116 (2004).

[6] Lin, H., Zhang, L., Li, L., Jin, Ch., Zhou, H. and Huo, T., "High-efficiency multilayer-coated ion-beam-etched blazed grating in the extreme-ultraviolet wavelength region", Opt. Lett. 33(5), 485-487 (2008).

[7] Bae, S.-E., Oh, M.-K., Min, N.-K., Paek, S.-H., Hong, S.-I. and Lee, Ch.-W. J., "Preparation of Atomically Flat Si(111)-H Surfaces in Aqueous Ammonium Fluoride Solutions Investigated by Using Electrochemical, *In Situ* EC-STM and ATR-FTIR Spectroscopic Methods," Bull. Korean Chem. Soc. 25(12), 1822-1828 (2004).

[8] Philippe, P., Valette, S., Mata Mendez, O. and Maystre, D., "Wavelength demultiplexer: using echelette gratings on silicon substrate, " Appl. Opt. 24(7), 1006-1011 (1985).

[9] Franke, A. E., Schattenburg, M. L., Gullikson, E. M., Cottam, J., Kahn, S. M. and Rasmussen. A., "Super-smooth x-ray reflection grating fabrication," J. Vac. Sci. Technol. B 15(6), 2940-2945 (1997).

[10] Underwood, J. H., Malek, C. Kh., Gullikson, E. M. and Krumrey, M., "Mdtilayer-coated echelle gratings for soft x rays and extreme ultraviolet, " Rev. Sci. Instrum. 66(2), 2147-2150 (1995).

[11] Ahn, M., Heilmann, R. K. and Schattenburg, M. L., "Fabrication of 200 nm period blazed transmission gratings on silicon-on-insulator wafers, " J. Vac. Sci. Technol. B 26(6), 2179-2182 (2008).

[12] Heilmann, R. K., Chen, C. G., Konkola, P. T. and Schattenburg M. L., "Dimensional metrology for nanometre-scale science and engineering: towards sub-nanometre accurate encoders," Nanotechnology 15(10), S504-S511 (2004).

[13] Rife, J. C., Barbee, Jr., T. W., Hunter, W. R. and Cruddace, R. G., "Performance of a Tungsten/Carbon Multilayer-Coated, Blazed Grating from 150 to 1700eV, " Physica Scripta 41, 418-421 (1990).
[14] Salmassi, F., Naulleau, P. P., Gullikson, E. M., Olynick, D. L. and Liddle, J. A., "Extreme ultraviolet binary phase gratings: Fabrication and application to diffractive optics," J. Vac. Sci. Technol. A 24(4), 1136-1140 (2006).
[15] Wind, R. A. and Hines, M. A., "Macroscopic etch anisotropies and microscopic reaction mechanisms: a micromachined structure for the rapid assay of etchant anisotropy," Surf. Science 460, 21–38 (2000).
[16] Voronov, D. L., Cambie, R., Gullikson, E. M., Yashchuk, V. V., Padmore, H. A., Pershin, Yu. P., Ponomarenko, A. G. and Kondratenko, V. V., "Fabrication and characterization of a new high density Sc/Si multilayer sliced grating," Proc. SPIE 7077, 707708-1 - 707708-12 (2008).
[17] Xiao, Z., Xu, M., Ohgi, T., Onishi, K. and Fujita, D., "Removal of Si(1 1 1) wafer surface etch pits generated in ammonia-peroxide clean step, " Appl. Surf. Science 221, 160–166 (2004).
[18] Voronov, D. L., Cambie, R., Feshchenko, R. M., Gullikson, E. M., Padmore, H. A., Vinogradov, A. V. and Yashchuk, V. V., "Development of an ultra-high resolution diffraction grating for soft X-rays," Proc. SPIE 6705, 67050E (2007).
[19] Levashov, V. E., Zubarev, E. N., Fedorenko, A. I., Kondratenko, V. V., Poltseva, O. V., Yulin, S. A., Struk, I. I. and Vinogradov, A. V., "High throughput and resolution compact spectrograph for the 124-250A range based on MoSi2-Si sliced multilayer grating, " Opt. Comm. 109, 1-4 (1994).
[20] Fechtchenko, R. M., Vinogradov, A. V., Voronov, D. L., "Optical properties of sliced multilayer gratings," Opt. Comm. 210, 179-186 (2002).